3D IMAGING OF ICE SHEETS

John Paden[1], Chris Allen[2], Prasad Gogineni[2]

[1]Vexcel Corporation, 5775 Flatiron, Suite 220, Boulder, CO 80301, USA
[2]Center for Remote Sensing of Ice Sheets and EECS Department, The University of Kansas, 2335 Irving Hill Road, Lawrence, KS 66045, USA

1. INTRODUCTION

We developed and deployed, in July 2005, a wideband 8-channel synthetic aperture radar (SAR) at Summit Camp, Greenland (72.5783° N and 38.4596° W). The nadir-looking radar was designed to map internal layers, measure topography, and generate backscatter maps – all in a single pass [1]. All of these data outputs can be used to refine glaciological models of ice sheets for predicting ice-sheet behavior (especially mass balance) and for selecting deep ice- core sites. This work focuses on the use of fine-resolution 3D imaging algorithms for combing the 8-channels to form cross-track image slices through the ice. As compared with traditional 2D depth sounding, these 3D images allow for characterizing bed topography with fine resolution. They also allow the generation of strip-map SAR images with absolute geocoding without ground control points (which are unavailable at the bottom of the ice), and the ability to analyze the ice-sheet volume in 3D. Topography, backscattering, and 3D ice volume results are illustrated here.

2. BACKGROUND

Traditional SAR imaging resolves a target's range, R and azimuth angle (doppler), θ, as shown in Fig. 1. For a monostatic-radar with a straight flight-line system, the isodoppler and isorange contours intersect on a circle rather than a single point. A target's 3D position is constrained to this circle and its position is not precisely known. Multiple channels in the cross-track dimension (either through multi-pass collections or with an antenna array) allow direction of arrival estimation and beam forming methods to be applied to resolve the circle of ambiguity to a single point. With the recent addition of multichannel radar systems to the field of radioglaciology, true 3D imaging is possible. This allows fine-resolution digital elevation maps and SAR images to be generated. A new and exciting avenue is the possibility to generate 3D images of structures within the ice.

With the Summit Camp, Greenland data collected with the 8-channel nadir-looking radar we start by framing the 3D imaging problem along two separate paths: locating targets and estimating their backscatter [1]. This framing allows us to choose estimators designed to minimize the error for the parameter of interest.

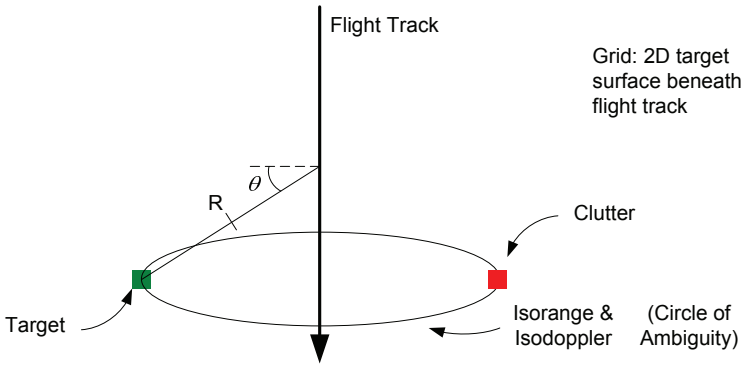

Fig. 1. Traditional 2D imaging geometry.

Locating the targets suggests the use of parametric direction of arrival estimation routines. As described by Van Trees, the optimal algorithm combines a number of targets estimate with a maximum likelihood estimator (MLE) of the direction of arrival for each of these targets, [2]. Due to the computational complexity of this optimal approach, we have started with the assumption of two targets and the use of quadratic Minimum Variance Distortionless Response (MVDR) and Eigen-based MUltiple SIgnal Classification, (MUSIC) approximations to this MLE. The justification for two targets relies on the use of formed SAR imagery and the assumption that we are measuring a 2D surface in a 3D volume (rather than a truly random distribution of targets). The 2D surface only intersects the circle of ambiguity in two places as shown in Fig. 1.

For estimating the backscatter response we make use of the minimum mean squared error based algorithm—MVDR or Capone method. This method allows for improved performance over the traditional matched filter because it adaptively adjusts the filter weights to reduce clutter energy– which is quite effective when clutter is restricted, in a linear algebra sense, to a small subspace of the total measurement space.

We show 3D cross-track image slices using the periodogram, MVDR, and MUSIC in Fig. 2. All three algorithms allow the combination of independent measurements. Neighboring pixels in the SAR image are used for these independent measurements. The assumption is that the target structure in this neighborhood is sufficiently smooth to assume that the scattering is stationary. Five range lines and three range bins centered on the pixel of interest are used. This leads to 15 independent measurements from the 8-channel array.

The periodogram incoherently averages the Fourier spectrum from each of the independent measurements available [2]. Both MVDR and MUSIC algorithms start by estimating the 8-channel array's covariance matrix. For a given along-track index, x, and range index ρ, there are eight measurements, one taken from each of the eight-receive-antennas. Let the vector $\bar{x}_{x,\rho}$ represent these eight measurements. We then create a matrix from the 15 independent measurements: $\bar{\bar{X}} = \left[\bar{x}_1 \middle| \bar{x}_2 \middle| \cdots \middle| \bar{x}_{15}\right]$. The autocorrelation matrix is then estimated by $\bar{\bar{R}}_{XX} = \bar{\bar{X}}\bar{\bar{X}}^H$.

MVDR can be simplified by combining the estimation of the autocorrelation matrix, the application of the filter coefficients, and the incoherent mean of the results. The simplified result is $\frac{1}{s^H \overline{\overline{R}}_{XX}^{-1} s}$ where $s = \left[1 \; e^{j2\pi F} \; e^{j2\cdot 2\pi F} \cdots e^{j(M-1)2\pi F}\right]$ is the steering vector for the normalized spatial frequency, F, that we are estimating a return for [2].

For the MUSIC algorithm, the eigenvectors, $\overline{\overline{V}}_{x,\rho}$, and eigenvalues for the matrix $\overline{\overline{R}}_{XX}$ are found [2]. Let $\bar{v}_{i,x,\rho}$ be the i^{th} eigenvector and also let the eigenvectors be sorted according to the size of their corresponding eigenvalues so that $\bar{v}_{1,x,\rho}$ has the largest eigenvalue and $\bar{v}_{8,x,\rho}$ has the smallest eigenvalue. The pseudospectrum is then given by $P(F) = \frac{1}{\sum_{i=p+1}^{M} \left| s^H v_i \right|^2}$ where $p = 2$ is the number of expected targets, and $M = 8$ is the number of samples per measurement.

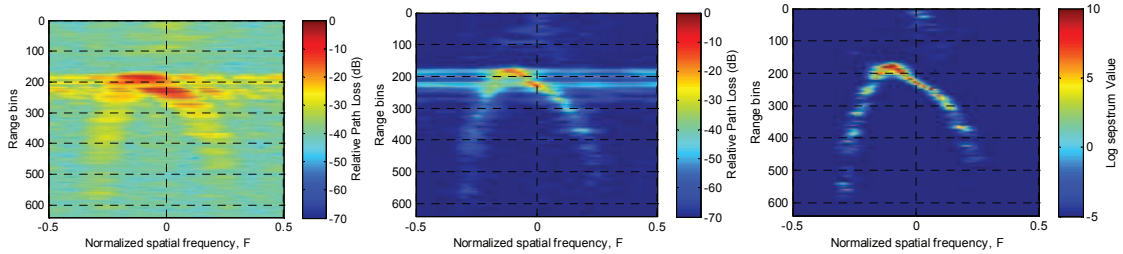

Fig. 2. From left to right, 3D image slices using periodogram, MVDR, and MUSIC.

3. RESULTS

Fig. 3 below shows the use of the algorithms to investigate 3D ice volumes. It shows that the deep internal layers (range bins 0-600) are very smooth and only generate a specular response at nadir, zero spatial frequency. However, near the bottom at range bin 850, the slopes of the internal layers become great enough that interesting patterns form near the base – following the theory that the ice-sheet layer structures are low-pass filtered versions of the bed topography with the cutoff frequency gradually going to zero the further from the bed the layer is.

Fig. 4 below shows the result of using the MUSIC algorithm to estimate the topography from the base of the ice sheet after using an ice sheet propagation model to geocode the results [3]. The cross-track width of the topography swath is 1600 m or 800 m on each side of the radar.

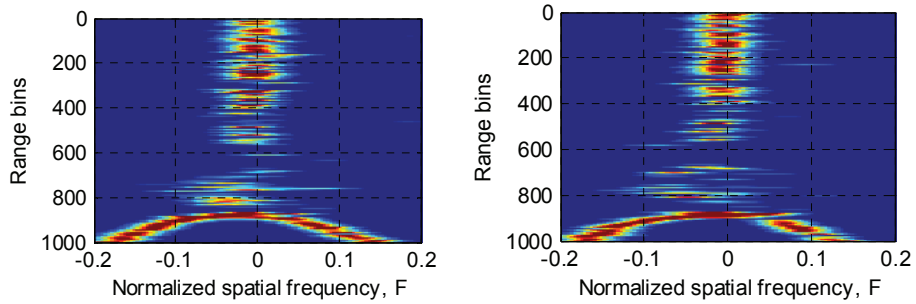

Fig. 3. Consecutive MUSIC generated 3D slices showing disturbed bottom internal layers. The colorbar scale is log sepstrum and ranges from -5 to +5.

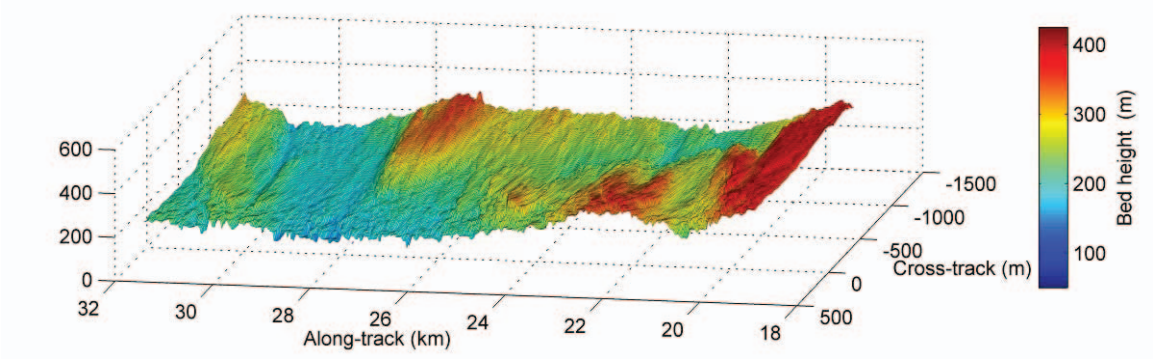

Fig. 4. DEM from a single pass using the MUSIC algorithm.

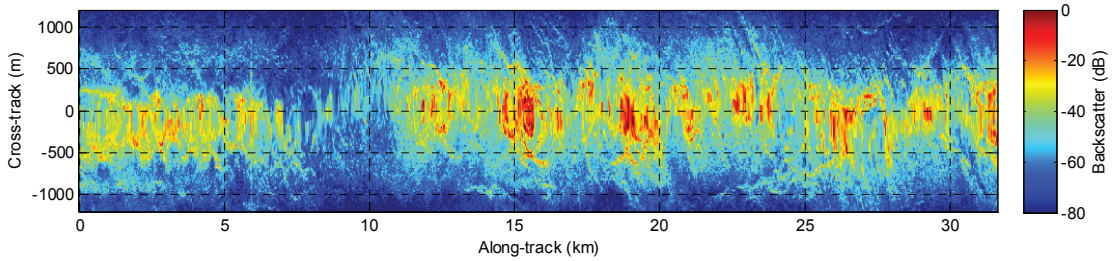

Fig. 5. Relative backscatter from a single pass using the MVDR algorithm.

Fig. 5 shows the use of the topographic estimate to generate a backscatter map using the MVDR algorithm. The resolution is finest on the edges where it is set by the range resolution (80 MHz) and degrades toward nadir where it is set by the 8-channel array. The cross-track swath width is 2400 m or 1200 m on each side of the radar.

[1] C. Allen, J. Paden, D. Dunson, and S. Gogineni, "Ground-based multi-channel SAR for mapping the ice-bed interface," *2008 IEEE Radar Conference*, pp. 1428-1433, *26-29 May 2008*.

[2] Harry L. Van Trees, *Optimum Array Processing (Detection, Estimation, and Modulation Theory, Part IV)*, Wiley, New York, Chapter 8-9, 2002.

[3] J. Paden, T. Akins, D. Dunson, C. Allen, and S. Gogineni, "Ice Sheet Bed 3D Tomography," *Journal of Glaciology*, accepted for publication, Jan 2010.